PERGAMON

International Journal of Solids and Structures 37 (2000) 4103–4124

INTERNATIONAL JOURNAL OF SOLIDS and STRUCTURES

www.elsevier.com/locate/ijsolstr

An elastodynamic hybrid boundary element study for elastic guided wave interactions with a surface breaking defect

Younho Cho[a], Joseph L. Rose[b,*]

[a]*School of Mechanical and Automotive Engineering, Inje University, 607, Obang-Dong, Kimhae, Kyongnam, 621-749, Republic of Korea*
[b]*The Pennsylvania State University, Ultrasonics R&D Center, Department of Engineering Science and Mechanics, 114A Hallowell Building, University Park, PA 16802, USA*

Received 24 October 1998; in revised form 31 October 1998

Abstract

Elastic guided wave interactions with various defects are explored for investigating defect characterization possibilities by using a hybrid boundary element method (BEM) in combination with an elastodynamic boundary integral equation and the Lamb wave normal mode expansion technique. The BEM code accuracy is verified based on energy conservation and available bench marking data for guided wave scattering problems. Through two-dimensional (2-D) parametric studies for an arbitrarily shaped defect, from a surface breaking crack model to a round surface defect, a waveguide cross-section including a defect is locally selected as a model for a given incident mode, frequency and a specific set of material properties. Mode reflection and transmission factors are numerically calculated to evaluate mode sensitivities and to obtain the potentially good classification features. It turns out that the guided wave scattering profiles show quite different behaviors as functions of incident mode, frequency, defect shape and size in providing us with enough rich feature extraction information for defect classification and sizing analysis. The theoretical analysis can be used to establish efficient guidelines for both data acquisition and feature selection in a pattern recognition analysis program of study. Sample results are presented.

Keywords: Guided wave; Boundary element method; Scattering; Surface defect

1. Introduction

Elastodynamic studies on elastic wave propagation in solid media have great importance in solid

* Corresponding author. Tel.: +1-814-863-8026; fax: +1-814-863-8164.
E-mail address: jlresm@engr.psu.edu (J.L. Rose).

0020-7683/00/$ - see front matter
PII: S0020-7683(99)00142-0

mechanics and structural analysis in helping us understand the dynamic response of the media. This work is particularly useful in the ultrasonic nondestructive evaluation field, which is based on the use of elastic waves. Investigations of elastic wave propagation and scattering is inevitable, if one is to interpret correctly a signal from a scatterer. In wave mechanics, it is a well-known fact that interference among the large numbers of longitudinal and transverse modes reflected from a thin structural boundary can generate elastic guided wave modes propagating along a particular geometry (Lamb, 1889; Viktorov, 1967; Achenbach, 1975). A guided wave generated in a plate-like structure is called a Lamb wave. This occurs when an incident wavelength is comparable to structure thickness.

Over the last decade, the use of guided waves for inspecting large structures has been of great concern to many elastic wave researchers due to both the potential for a more sensitive and faster inspection. Hence, there have been vigorous attempts to investigate various guided wave aspects for NDE purposes (Rose et al., 1994; Cho and Rose, 1996a). However, complicated mode conversion phenomena in guided wave scattering problems can be potentially useful in establishing key features in quantitative guided wave inspection for defect classification and sizing. Compared to conventional boundary value problems for guided wave propagation, theoretical analysis of guided wave scattering from defects is extremely difficult because of the complex multi-mode conversion phenomena and arbitrary shaped boundary and defect geometries. Unlike elastic bulk wave scattering, guided wave scattering involves not only the scattering of an incident mode but also those of all other possible propagating modes existing at a certain frequency through mutual interference. Therefore, studies on guided wave scattering problems are relatively rare (Cho and Rose, 1996b; Auld and Tsao, 1977; Rokhlin, 1980; Koshiba et al., 1984; Zhang et al., 1988; Datta et al., 1991; Al-Nassar et al., 1991; Alleyne and Cawley, 1992; Karim et al., 1992), compared to the more well-known bulk wave scattering problems (Schafbuch et al., 1993; Kobayashi 1987; Rizzo et al., 1985; Zhang and Achenbach, 1988; Rezayat et al., 1986). Hence, multi-mode conversion phenomena found in a Lamb wave interaction with a defect is still not fully understood.

Recently, the authors presented the various mode conversion curves of a Lamb wave edge reflection in a steel plate by the hybrid BEM (Cho and Rose, 1996b). According to the edge reflection BEM study (Cho and Rose, 1996b), it was proven that the hybrid BEM can be successfully applied to guided wave scattering and readily extended to guided wave scattering from a defect with improved numerical efficiency over domain type techniques.

The Lamb wave mode conversion from arbitrary defects has been studied both theoretically and numerically (Rokhlin, 1980; Koshiba et al., 1984; Datta et al., 1991; Al-Nassar et al., 1991, Alleyne and Cawley, 1992; Karim et al., 1992). An adequate theoretical and numerical analysis of the propagation and scattering of ultrasonic waves is essential for the optimization of quantitative nondestructure testing and also for the development of new techniques. However, the range of pure theoretical solutions remains limited and many practical ultrasonic problems including guided wave scattering, are analytically unsolvable due to arbitrary boundary conditions and geometrical complexity (Achenbach, 1992; Bond, 1990). For this reason, a numerical approach has become a useful tool for solving ultrasonic scattering problems with the help of various numerical integration schemes. A comparison of the capabilities and limitations of the various numerical models can be found in some previous works (Brebbia et al., 1985; Achenbach, 1992; Bond, 1990).

As in other engineering problems, the finite element method (FEM) has been the most popular simulation technique for ultrasonic scattering because of the simplicity of the numerical formulation. Even in a guided wave problem, a numerical approach can become more powerful than in a bulk wave problem since a waveguide must be defined in a bounded domain, being closely associated with geometrical complexity. The boundary value problems for obtaining dispersion curves of either an

unusually shaped waveguide or a multi-layered waveguide were investigated with the aid of FEM (Talbot and Przemieniecki, 1975).

In 1984, Koshiba used FEM for solving fundamental symmetric Lamb wave scattering problems in an elastic plate and confirmed the validity of the use of FEM by comparing numerical results with analytical solutions of a Variation Method (Koshiba et al., 1984). He considered only symmetric propagating modes in a simply shaped waveguide joint. Al-Nassar et al. calculated reflection and transmission factors of scattered fields due to a normal rectangular strip weldment in a plate by FEM (Al-Nassar et al., 1991). Alleyne and Cawley combined time domain FEM solutions with Fourier transform methods to quantify Lamb wave scattered fields (Alleyne and Cawley, 1992). The scattering of elastic waves in a plate by inclusions was studied within a finite zone by a solution matching technique of the hybrid FEM between a near and a far field (Karim et al., 1992).

Even though FEM has been used broadly for elastodynamic problems, it sometimes requires a greater effort for mesh generation and computing time than boundary type simulation techniques, due to the nature of its domain type formulation. Consequently, it is sometimes very tedious to apply FEM to more complex shaped waveguide problems. However, most of the previous studies on Lamb wave interactions with a defect were based on the use of the FEM (Talbot and Przemieniecki, 1975; Koshiba et al., 1984; Datta et al., 1991; Al-Nassar et al., 1991; Alleyne and Cawley, 1992; Karim et al., 1992). Also, focus has been on investigating a scattering profile from a fixed defect type rather than comparing differences in scattering patterns with respect to defect shape change, say defect sharpness for the purpose of defect characterization. Therefore, efficient and advanced numerical methods are needed for studies of guided wave scattering and defect characterization in a waveguide.

Recently, advantages of the boundary integral equation method over other domain type modeling techniques were discussed by many researchers (Brebbia et al., 1985; Achenbach, 1992; Bond, 1990). The technique has been broadly used in solving various bulk wave scattering problems (Schafbuch et al., 1993; Kobayashi, 1987; Rizzo et al., 1985; Zhang and Achenbach, 1988; Rezayat et al., 1986). Even though there were many BEM studies in elastodynamics, most were limited to cases of bulk wave scattering rather than guided wave applications. As far as the authors know, boundary element works related to guided wave scattering problems are rare. Recently, the authors proposed the hybrid BEM based on a combination of elastodynamic interior boundary integral equations and the Lamb wave normal mode expansion technique for the Lamb wave edge reflection study (Cho and Rose, 1996b).

The boundary element formulation is mathematically more sophisticated than the FEM due to the singularities of the corresponding fundamental solutions (Brebbia et al., 1985; Kobayashi, 1987; Brebbia et al., 1984). However, once the singular integration schemes of the fundamental solution is achieved (Kobayashi, 1987; Kitahara et al., 1989; Rezayat et al., 1986; Lachat and Watson, 1976; Brebbia et al., 1984), the BEM can be a more efficient numerical technique over a domain type technique. It can easily manage unbounded domains and bounded domains of arbitrary geometry just by simply discretizing a boundary and not a whole domain. In this paper, the hybrid BEM used in the edge reflection study (Cho and Rose, 1996b) is applied in analyzing Lamb wave interactions with surface defects with different sharpness and depth. Artificial elliptical defects were also constructed in order to represent surface wastage while rectangular defects were constructed to represent surface open breaking defects. The reflection and transmission factors are numerically calculated as a function of incident mode, defect sharpness and depth, in order to evaluate mode sensitivity and to obtain physical information for Lamb wave mode conversion. The practical purpose of the work is to eventually optimize data collection procedures via proper mode input in order to tackle the inverse problem of defect classification and sizing.

2. Theoretical background

2.1. The conventional elastodynamic interior boundary integral formulation

From Fig. 1, the elastodynamic interior boundary integral equation of a modeling zone in a plate can be derived from the equation of motion through a weighted residual method as follows (Kobayashi, 1987; Brebbia et al., 1984),

$$c_{ki}(\bar{\xi})u_i(\bar{\xi}) + \int_\Gamma t^*_{ki}(\bar{\xi}, \bar{\chi})u_i \, \mathrm{d}\Gamma = \int_\Gamma u^*_{ki}(\bar{\xi}, \bar{\chi})t_i \, \mathrm{d}\Gamma \quad \text{on } \Gamma \tag{1}$$

where $c_{ki} = 1/2$, if the boundary Γ is smooth, u_i and t_i denote surface displacement and traction, respectively.

The displacement and traction fundamental solution, u^*_{ki} and t^*_{ki} of a Fourier transformed elastodynamic domain are given as follows (Kobayashi, 1987; Brebbia et al., 1984),

$$u^*_{ki}(\xi, \chi) = A(\hat{U}_1\delta_{ki} - \hat{U}_2 r_{,\,k} r_{,\,i}) \tag{2}$$

$$t^*_{ki}(\xi, \chi) = GA\left[\left\{\left(\delta_{ki}\frac{\partial r}{\partial n} + n_k r_{,\,i}\right) + \frac{\lambda}{G} + n_i r_{,\,k}\right\}\frac{\mathrm{d}\hat{U}_1}{\mathrm{d}r} - \left\{\left(\delta_{ki}\frac{\partial r}{\partial n} + n_k r_{,\,i}\right) + 2\left(n_{,\,i} r_{,\,k} - 2r_{,\,k} r_{,\,i}\frac{\partial r}{\partial n}\right) + \alpha\frac{\lambda}{G} n_i r_{,\,k}\right\}\frac{\hat{U}_2}{r} - \left\{2r_{,\,k} r_{,\,i}\frac{\partial r}{\partial n} + \frac{\lambda}{G} n_i r_{,\,k}\right\}\frac{\mathrm{d}\hat{U}_2}{\mathrm{d}r}\right] \tag{3}$$

where a position vector between a unit point load and a field point and coefficients α and A are defined as follows

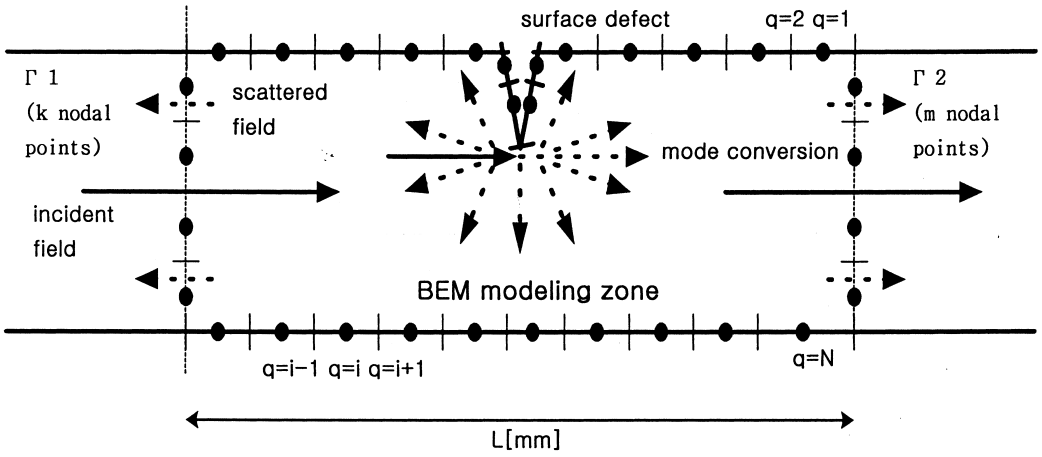

Fig. 1. The hybrid BEM modeling zone with constant elements in a plate.

$$|\bar{r}| = |\bar{\xi} - \bar{\chi}| \quad \alpha = 1(\text{for } 2D) \quad A = i/4G(\text{for } 2D)$$

The fundamental vectors in (2) and (3) are,

$$\hat{U}_1 = H_0^{(1)}(k_T r) - \frac{1}{k_T r} H_1^{(1)}(k_T r) + \left(\frac{k_L}{k_T}\right)^2 \frac{1}{k_L r} H_1^{(1)}(k_L r) \tag{4}$$

$$\hat{U}_2 = -H_2^{(1)}(k_T r) + \left(\frac{k_L}{k_T}\right)^2 H_2^{(1)}(k_L r) \tag{5}$$

where k_L is the longitudinal wave number, k_T the transverse wave number and $H_1^{(1)}$ and $H_2^{(1)}$ are the Hankel functions of the first kind of order 1 and 2, respectively.

Discretizing the boundary Γ with N constant elements as shown in Fig. 1 (for the pth element)

$$\begin{bmatrix} \frac{1}{2} & 0 \\ 0 & \frac{1}{2} \end{bmatrix} \begin{Bmatrix} u_{2q-1} \\ u_{2q} \end{Bmatrix} = \sum_{q=1}^{N} \int_{\Gamma_q} \begin{bmatrix} u^*_{2p-1,\,2q-1} & u^*_{2p-1,\,2q} \\ u^*_{2p,\,2q-1} & u^*_{2p,\,2q} \end{bmatrix} \begin{Bmatrix} t_{2q-1} \\ t_{2q} \end{Bmatrix} d\Gamma_q - \sum_{q=1}^{N} \int_{\Gamma_q} \begin{bmatrix} t^*_{2p-1,\,2q-1} & t^*_{2p-1,\,2q} \\ t^*_{2p,\,2q-1} & t^*_{2p,\,2q} \end{bmatrix} \times \begin{Bmatrix} u_{2q-1} \\ u_{2q} \end{Bmatrix} d\Gamma_q \tag{6}$$

($p = 1, 2, 3, \ldots, N$).

The eight-point Gaussian quadrature procedure is used for the off-diagonal regular numerical integration and the Cauchy principal value is analytically calculated for the diagonal singular integration, respectively (Kobayashi, 1987; Kitahara et al., 1989; Rezayat et al., 1986; Lachat and Watson, 1976; Brebbia et al., 1984). Eq. (6) can also be expressed in terms of matrix notation through the matrix globalization by changing a point loading location over the entire waveguide boundary Γ,

$$HU = GT \quad \text{on } \Gamma \tag{7}$$

where U and T are the boundary total displacement and traction vector. H and G are the boundary integral terms of the traction and displacement fundamental solutions.

2.2. Hybrid boundary element formulation for a Lamb wave scattering problem

In an elastic waveguide, the incident displacement field u^I of the pth mode propagating along the positive x_1-axis can be expressed in terms of amplitude α^p, the normalized displacement model function u^p and pth wave number k^p by factoring out the time harmonic term,

$$u^I = u^p = \alpha^p \bar{u}^p = \alpha^p \begin{Bmatrix} \bar{u}^p_{x_1} \\ \bar{u}^p_{x_2} \end{Bmatrix} e^{ik^p x_1} \tag{8}$$

The normalized modal displacement and traction functions can be obtained from the boundary value problem of the Lamb wave propagation (Viktorov, 1967; Achenbach, 1975; Cho and Rose, 1996b). The Lamb wave modal functions for symmetric and anti-symmetric modes derived through the eigenvector problem of a plate are as follows,

(symmetric mode)

$$\hat{u}_{x_1} = \frac{u_{x_1}}{A_1} = [ik \ \cos \ k_l x_2 + k_t \alpha \ \cos \ k_t x_2] e^{i(kx_1 - \omega t)} \tag{9}$$

$$\hat{u}_{x_2} = \frac{u_{x_2}}{A_1} = [-k_l \ \sin \ k_l x_2 - ik\alpha \ \sin \ k_t x_2] e^{i(kx_1 - \omega t)} \tag{10}$$

$$\hat{\sigma}_{x_1 x_1} = \frac{\sigma_{x_1 x_1}}{A_1} = [\{-\lambda(k^2 + k_l^2) - 2Gk^2\} \cos \ k_l x_2 + 2Gikk_t \alpha \ \cos \ k_t x_2] e^{i(kx_1 - \omega t)} \tag{11}$$

$$\hat{\sigma}_{x_1 x_2} = \frac{\sigma_{x_1 x_2}}{A_1} = [-2Gikk_l \ \sin \ k_l x_2 + G(k^2 - k_t^2)\alpha \ \sin \ k_t x_2] e^{i(kx_1 - \omega t)} \tag{12}$$

(anti-symmetric mode)

$$\hat{u}_{x_1} = \frac{u_{x_1}}{A_2} = [ik \ \sin \ k_l x_2 - k_t \beta \ \sin \ k_t x_2] e^{i(kx_1 - \omega t)} \tag{13}$$

$$\hat{u}_{x_2} = \frac{u_{x_2}}{A_2} = [k_l \ \cos \ k_l x_2 - ik\beta \ \cos \ k_t x_2] e^{i(kx_1 - \omega t)} \tag{14}$$

$$\hat{\sigma}_{x_1 x_1} = \frac{\sigma_{x_1 x_1}}{A_2} = [\{-\lambda(k^2 + k_l^2) - 2Gk^2\} \sin \ k_l x_2 - 2Gikk_t \beta \ \sin \ k_t x_2] e^{i(kx_1 - \omega t)} \tag{15}$$

$$\hat{\sigma}_{x_1 x_2} = \frac{\sigma_{x_1 x_2}}{A_2} = [2Gikk_l \ \cos \ k_l x_2 + G(k^2 - k_t^2)\beta \ \cos \ k_t x_2] e^{i(kx_1 - \omega t)} \tag{16}$$

and

$$\alpha = \frac{A_4}{A_1} = \frac{2ikk_l \ \sin \ k_l d/2}{(k^2 - k_t^2) \sin \ k_t d/2} \tag{17}$$

$$\beta = \frac{A_3}{A_2} = \frac{-2ikk_l \ \cos \ k_l d/2}{(k^2 - k_t^2) \cos \ k_t d/2} \tag{18}$$

Consequently, the normalized modal functions for the nth propagating mode are calculated based on the ratio of the square root of an in-plane average power between the mode and an incident mode (Viktorov, 1967; Achenbach, 1975; Cho and Rose, 1996a, b),

$$\bar{U}_{x_1}^n = N_I^n \times \hat{u}_{x_1}^n \tag{19}$$

$$\bar{U}_{x_2}^n = N_I^n \times \hat{u}_{x_2}^n \tag{20}$$

$$\bar{\sigma}_{x_1 x_1}^n = N_I^n \times \hat{\sigma}_{x_1 x_1}^n \tag{21}$$

$$\bar{\sigma}_{x_1 x_2}^n = N_I^n \times \hat{\sigma}_{x_1 x_2}^n \tag{22}$$

where N_I^n denotes the normalized factor based on the power ratio between the nth mode and an incident

mode and the in-plane average power (Viktorov, 1967; Achenbach, 1975; Cho and Rose, 1996a, b) is,

$$N_{\mathrm{I}}^{n} = \sqrt{\frac{\bar{P}_{x_1}^{\mathrm{I}}}{\bar{P}_{x_1}^{n}}} \tag{23}$$

$$\bar{P}_{x_1} = -\frac{1}{2}\mathrm{real}\left[-i\omega \int_{-d/2}^{d/2} \{\hat{\sigma}_{x_1x_1}\hat{u}_{x_1} + \hat{\sigma}_{x_1x_2}\hat{u}_{x_2}\}\mathrm{d}x_2 \right] \tag{24}$$

Then, the normalized surface traction t can be defined as the product of the outward normal n on a boundary and the stress modal functions.

The scattered field induced by the pth incident wave mode could contain J and L numbers of independent normal modes on the left and right boundaries, Γ_1 and Γ_2, respectively, at a certain frequency through the mode conversions on the scatterer surface. These modes can be found in the dispersion curves of Fig. 2. For example, at fd = 1.0 MHz mm, both J and L are 2, representing two independent propagating modes, A0 and S0. Therefore, under the assumption of an isotropic linear elastic waveguide, they can be linearly superposed to express the resulting scattered fields in elastic waveguides with geometrical discontinuities in the following manner:

$$u^{\mathrm{BS}} = \sum_{j=1}^{J} \beta^{j}\bar{u}^{j} = \sum_{j=1}^{J} \beta^{j} \begin{Bmatrix} \bar{u}_{x_1}^{j} \\ \bar{u}_{x_2}^{j} \end{Bmatrix} \mathrm{e}^{-ik^{j}x_1} \quad \text{(backward scattering on } \Gamma_1\text{)} \tag{25}$$

$$u^{\mathrm{FS}} = \sum_{l=1}^{L} \beta^{l}\bar{u}^{l} = \sum_{l=1}^{L} \beta^{l} \begin{Bmatrix} \bar{u}_{x_1}^{l} \\ \bar{u}_{x_2}^{l} \end{Bmatrix} \mathrm{e}^{ik^{l}x_1} \quad \text{(forward scattering on } \Gamma_2\text{)} \tag{26}$$

Where the superscripts, 'BS' and 'FS', denote the back and forward scattering and β^{j} and β^{l} are the jth mode reflected and the lth transmitted amplitudes on Γ_1 and Γ_2, respectively.

The total displacement field can be defined as the superposition of incident and scattered fields on Γ_1

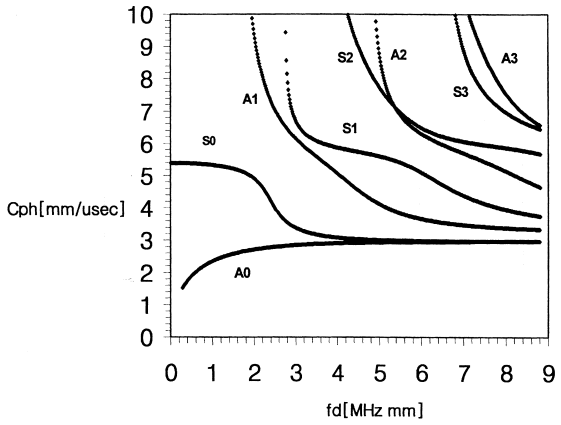

Fig. 2. The phase velocity dispersion curve of a steel plate.

and Γ_2

$$u = u^{\mathrm{I}} + u^{\mathrm{BS(FS)}} \quad \text{on } \Gamma_1(\text{on } \Gamma_2) \tag{27}$$

Discretizing Γ_1 and Γ_2 with k and m nodal points, respectively, as shown in Fig. 1, the following is obtained

$$\{u\}^{\Gamma_1}_{2k\times 1} = [\bar{u}]^{\mathrm{I}}_{2k\times J}\{\alpha^p\delta_{pj}\, \mathrm{e}^{ik^j x_1}\}_{J\times 1} + [\bar{u}]^{\mathrm{BS}}_{2k\times J}\{\beta^j\, \mathrm{e}^{-ik^j x_1}\}_{J\times 1} \quad \text{on } \Gamma_1 \tag{28}$$

$$\{u\}^{\Gamma_2}_{2m\times 1} = [\bar{u}]^{\mathrm{I}}_{2m\times L}\{\alpha^p\delta_{pl}\, \mathrm{e}^{ik^l x_1}\}_{L\times 1} + [\bar{u}]^{\mathrm{FS}}_{2m\times L}\{\beta^l\, \mathrm{e}^{ik^l x_1}\}_{L\times 1} \quad \text{on } \Gamma_2 \tag{29}$$

where

$$[\bar{u}]^{\mathrm{I,\ BS}} = \begin{bmatrix} \bar{u}^1_{x_1}(x_2^1) & \bar{u}^2_{x_1}(x_2^1) & \dots & \bar{u}^j_{x_1}(x_2^1) & \dots & \dots & \bar{u}^{J-1}_{x_1}(x_2^1) & \bar{u}^J_{x_1}(x_2^1) \\ \bar{u}^1_{x_2}(x_2^1) & \bar{u}^2_{x_2}(x_2^1) & \dots & \bar{u}^j_{x_2}(x_2^1) & \dots & \dots & \bar{u}^{J-1}_{x_2}(x_2^1) & \bar{u}^J_{x_2}(x_2^1) \\ \bar{u}^1_{x_1}(x_2^2) & \bar{u}^2_{x_1}(x_2^2) & \dots & \bar{u}^j_{x_1}(x_2^2) & \dots & \dots & \bar{u}^{J-1}_{x_1}(x_2^2) & \bar{u}^J_{x_1}(x_2^2) \\ \vdots & \vdots & \vdots & \vdots & \dots & \dots & \vdots & \vdots \\ \vdots & \vdots & \vdots & \vdots & \ddots & & \vdots & \vdots \\ \vdots & \vdots & \vdots & \vdots & & \ddots & \vdots & \vdots \\ \bar{u}^1_{x_1}(x_2^k) & \bar{u}^2_{x_1}(x_2^k) & \dots & \bar{u}^j_{x_1}(x_2^k) & \dots & \dots & \bar{u}^{J-1}_{x_1}(x_2^k) & \bar{u}^J_{x_1}(x_2^k) \\ \bar{u}^1_{x_2}(x_2^k) & \bar{u}^2_{x_2}(x_2^k) & \dots & \bar{u}^j_{x_2}(x_2^k) & \dots & \dots & \bar{u}^{J-1}_{x_2}(x_2^k) & \bar{u}^J_{x_2}(x_2^k) \end{bmatrix}_{2k\times J} \quad \text{on } \Gamma_1$$

and $[\bar{u}]^{\mathrm{FS}}$ can also be expressed in terms of m and L on Γ_2.

In a similar way, the total boundary tractions can be defined by a linear superposition of the normalized traction modal functions for the incident and scattered fields,

$$\{t\}^{\Gamma_1}_{2k\times 1} = [\bar{t}]^{\mathrm{I}}_{2k\times J}\{\alpha^p\delta_{pj}\, \mathrm{e}^{ik^j x_1}\}_{J\times 1} + [\bar{t}]^{\mathrm{BS}}_{2k\times J}\{\beta^j\, \mathrm{e}^{-ik^j x_1}\}_{J\times 1} \quad \text{on } \Gamma_1 \tag{30}$$

$$\{t\}^{\Gamma_2}_{2m\times 1} = [\bar{t}]^{\mathrm{I}}_{2m\times L}\{\alpha^p\delta_{pl}\, \mathrm{e}^{ik^l x_1}\}_{L\times 1} + [\bar{t}]^{\mathrm{FS}}_{2m\times L}\{\beta^l\, \mathrm{e}^{ik^l x_1}\}_{L\times 1} \quad \text{on } \Gamma_2 \tag{31}$$

where

$$[\bar{t}]^{\mathrm{I,\ BS}} = \begin{bmatrix} \bar{t}^1_{x_1}(x_2^1) & \bar{t}^2_{x_1}(x_2^1) & \dots & \bar{t}^j_{x_1}(x_2^1) & \dots & \dots & \bar{t}^{J-1}_{x_1}(x_2^1) & \bar{t}^J_{x_2}(x_2^1) \\ \bar{t}^1_{x_2}(x_2^1) & \bar{t}^2_{x_2}(x_2^1) & \dots & \bar{t}^j_{x_2}(x_2^1) & \dots & \dots & \bar{t}^{J-1}_{x_2}(x_2^1) & \bar{t}^J_{x_1}(x_2^1) \\ \bar{t}^1_{x_1}(x_2^2) & \bar{t}^2_{x_1}(x_2^2) & \dots & \bar{t}^j_{x_1}(x_2^2) & \dots & \dots & \bar{t}^{J-1}_{x_1}(x_2^2) & \bar{t}^J_{x_1}(x_2^2) \\ \vdots & \vdots & \vdots & \vdots & \dots & \dots & \vdots & \vdots \\ \vdots & \vdots & \vdots & \vdots & \ddots & & \vdots & \vdots \\ \vdots & \vdots & \vdots & \vdots & & \ddots & \vdots & \vdots \\ \bar{t}^1_{x_1}(x_2^k) & \bar{t}^2_{x_1}(x_2^k) & \dots & \bar{t}^j_{x_1}(x_2^k) & \dots & \dots & \bar{t}^{J-1}_{x_1}(x_2^k) & \bar{t}^J_{x_1}(x_2^k) \\ \bar{t}^1_{x_2}(x_2^k) & \bar{t}^2_{x_2}(x_2^k) & \dots & \bar{t}^j_{x_2}(x_2^k) & \dots & \dots & \bar{t}^{J-1}_{x_2}(x_2^k) & \bar{t}^J_{x_2}(x_2^k) \end{bmatrix}_{2k\times J} \quad \text{on } \Gamma_1$$

and $[\bar{t}]^{\mathrm{FS}}$ can also be expressed in terms of m and L on Γ_2.

Rearranging (28) and (29) with respect to the scattered amplitudes β^j and β^l,

$$\{\beta^j\, \mathrm{e}^{-ik^j x_1}\}_{J\times 1} = [\bar{u}^{-1}]^{\mathrm{BS}}_{J\times 2k}\{u\}^{\Gamma_1}_{2k\times 1} - [\bar{u}^{-1}]^{\mathrm{BS}}_{J\times 2k}[\bar{u}]^{\mathrm{I}}_{2k\times J}\{\alpha^p\delta_{pj}\, \mathrm{e}^{ik^j x_1}\}_{J\times 1} \quad \text{on } \Gamma_1 \tag{32}$$

$$\{\beta^l\, \mathrm{e}^{-ik^l x_1}\}_{L\times 1} = [\bar{u}^{-1}]^{\mathrm{FS}}_{L\times 2m}\{u\}^{\Gamma_2}_{2m\times 1} - [\bar{u}^{-1}]^{\mathrm{FS}}_{L\times 2m}[\bar{u}]^{\mathrm{I}}_{2m\times L}\{\alpha^p\delta_{pl}\, \mathrm{e}^{ik^l x_1}\}_{L\times 1} \quad \text{on } \Gamma_2 \tag{33}$$

where $[\bar{u}^{-1}]$ denoted the generalized complex inverse matrix of $[\bar{u}]$; $[\bar{u}^{-1}] = ([\bar{u}^*]^{\mathrm{T}}[\bar{u}])^{-1}[\bar{u}^*]^{\mathrm{T}}$ and $[\bar{u}^*]^{\mathrm{T}}$ denotes the transpose of the complex conjugate of $[\bar{u}]$ (Lancaster and Tismenetsky, 1985).

Substituting (32) and (33) into (30) and (31),

$$\{t\}^{\Gamma_1}_{2k\times 1} = [\bar{t}]^{\mathrm{I}}_{2k\times J}\{\alpha^p\delta_{pj}\, \mathrm{e}^{ik^j x_1}\}_{J\times 1} + [\bar{t}]^{\mathrm{BS}}_{2k\times J}[\bar{u}^{-1}]^{\mathrm{BS}}_{J\times 2k}\{u\}^{\Gamma_1}_{2k\times l} - [\bar{t}]^{\mathrm{BS}}_{2k\times J}[\bar{u}^{-1}]^{\mathrm{BS}}_{J\times 2k}[\bar{u}]^{\mathrm{I}}_{2k\times J}\{\alpha^p\delta_{pj}\, \mathrm{e}^{ik^j x_1}\}_{J\times 1} \quad \text{on } \Gamma_1 \tag{34}$$

$$\{t\}^{\Gamma_2}_{2m\times l} = [\bar{t}]^{\mathrm{FS}}_{2m\times L}[\bar{u}^{-1}]^{\mathrm{FS}}_{L\times 2m}\{u\}^{\Gamma_2}_{2m\times l} \quad \text{on } \Gamma_2 \tag{35}$$

Finally, we obtain $2k$ and $2\ m$ relations between boundary tractions and displacements on the left and right cross-sectional boundaries of a waveguide, respectively, instead of $2k$ and $2\ m$ boundary conditions. Substituting (34) and (35) into (7) and rearranging (7) with traction free boundary conditions on the top and bottom surfaces of a plate,

$$\{C\}_{2N\times 1} = [A]_{2N\times 2N}\{X\}_{2N\times 1} \tag{36}$$

where $\{C\}$ is the constant vector, $[A]$ is the coefficient matrix made of $[H]$ and $[G]$ matrices components and $\{X\}$ the unknown vector containing the boundary values of total boundary displacement fields, $\{u\}$.

When the total fields are obtained, the unknown backward and forward scattered amplitudes can be determined from (25) and (26). Consequently, the jth mode reflection and the lth mode transmission coefficients R^{jp} and T^{lp} can be calculated by dividing the scattered amplitudes by the pth incident amplitude, α^p

$$R^{jp} = \beta^j/\alpha^p \quad \text{on } \Gamma_1 \tag{37}$$

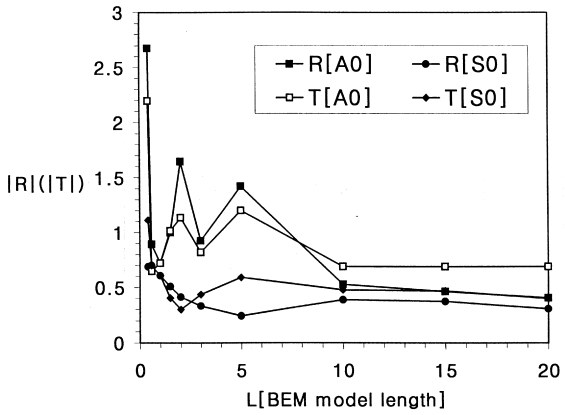

Fig. 3. BEM convergence test with respect to the model length L for A0 (fd = 1.5 MHz mm) incidence to a surface defect: L [mm].

$$T^{lp} = \beta^l/\alpha^p \quad \text{on } \Gamma_2 \tag{38}$$

where R^{jp} and T^{lp} are the jth mode reflection and the lth mode transmission coefficients induced by the pth incident Lamb wave mode.

2.3. Miscellaneous computation aspects

The BEM software is formulated in a 2-D frequency domain. The program also includes some auxiliary routines for auto meshing of the plate boundary and for wave structure calculations of both incident and scattered fields at a given frequency. The material properties for a steel used in the BEM simulations are the longitudinal wave velocity $C_L = 5.94$ mm/μs, the transverse wave velocity $C_T = 3.2$ mm/μs and density $\rho = 7.8$ g/cm^3. Plate thickness is fixed as one for convenience, so the input frequency represents directly a corresponding frequency time thickness value on the dispersion curve. To convince us of the accuracy of the technique based on the energy conservation concept, the error involved in the analysis can be estimated by the deviation of the total reflected and transmitted energies from the incident energy. Both constant and quadratic elements successfully represent analytical wave structures without any significant different in particle displacement calculations. Therefore, the constant element will be employed in further case studies.

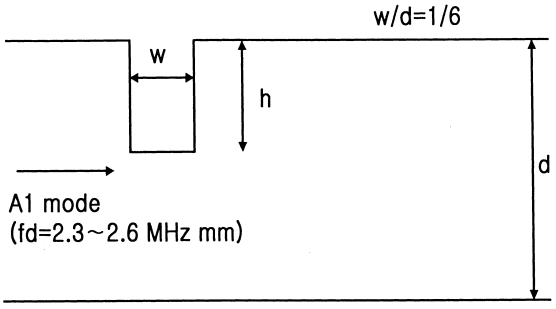

Fig. 4. The problem statement for A1 Lamb wave mode interaction with a square defect.

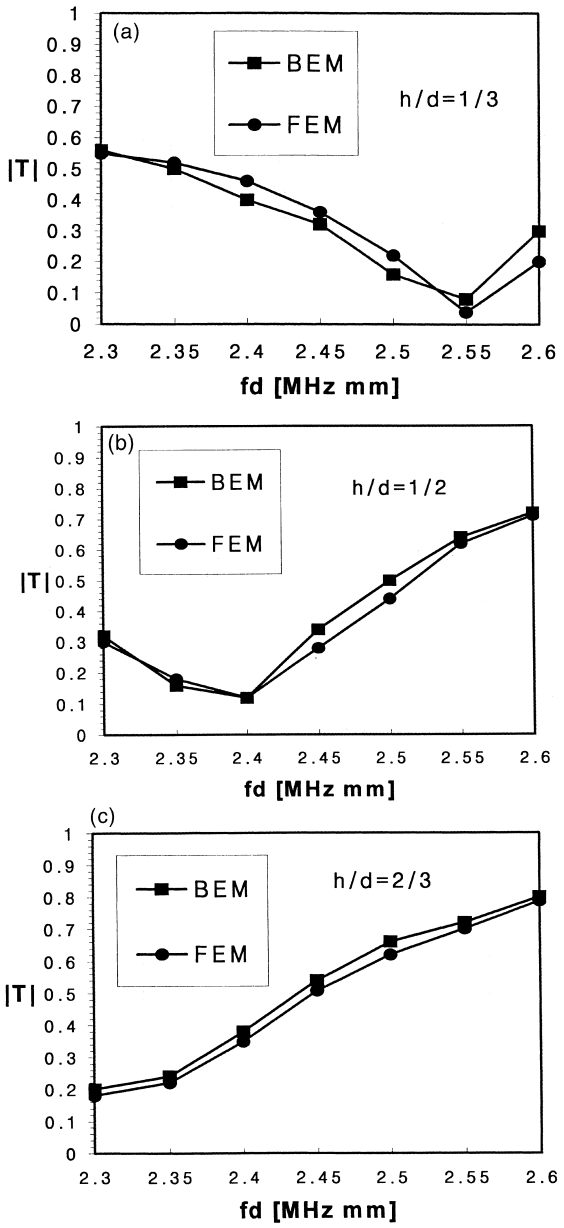

Fig. 5. A comparison between the BEM and the previous FEM studies (Alleyne and Cawley, 1992): (a) $h/d = 1/3$; (b) $h/d = 1/2$; (c) $h/d = 2/3$.

The distance between a reflector and cross-sectional boundaries can also be a critical factor in the accuracy of a hybrid formulation. Consequently, the model length L in Fig. 1 needs to be maintained long enough in order to meet the far field scattering conditions. Then, counting only the propagating modes with real wave numbers in linear superposition is sufficient for reasonable accuracy (Cho and Rose, 1996a, b; Koshiba et al., 1984; Karim et al., 1992). Fig. 3 represents the convergence of reflection

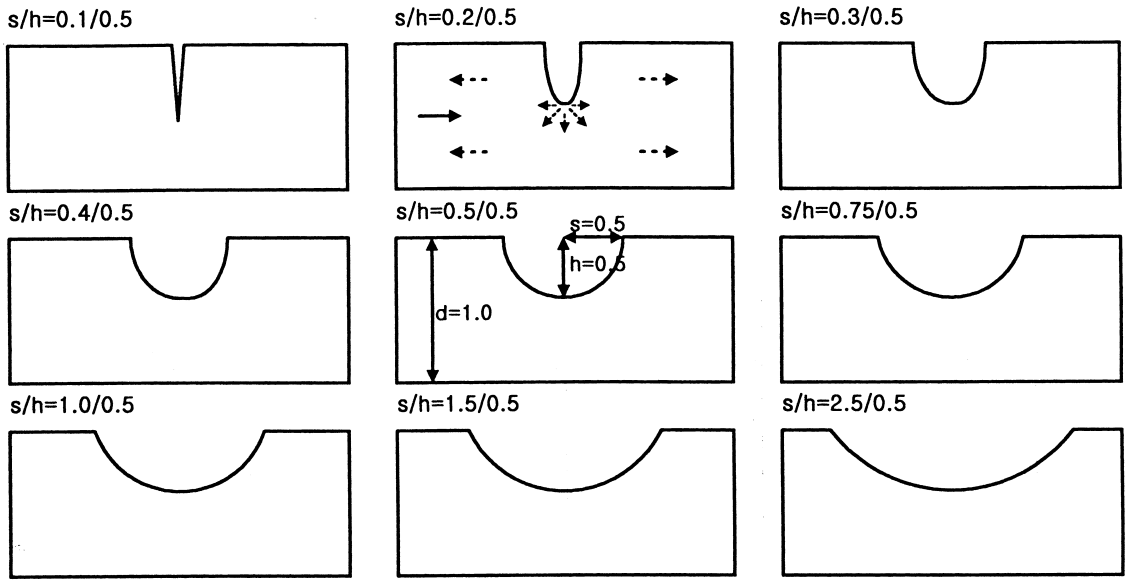

Fig. 6. A guided wave sensitivity study for variation of defect shape at a fixed incident frequency (incident mode: S0/A0 at fd = 1.0 MHz mm).

and transmission factors with an increase of the distance, $L/2$, between a reflector and the vertical cross-sectional boundary. With reasonable model length L, both reflection and transmission factors are nearly independent of the model size.

3. Numerical results and discussions

3.1. Comparison with the previous solutions for Lamb wave scattering

As a simple case of guided wave scattering, reflection from a free edge in a semi-infinite plate was already successfully solved by the present method (Cho and Rose, 1996a, b). It was found that the trend in all reflection factor curves of edge reflection were overall identical to that in the previous works for glass (Cho and Rose, 1996a, b). Also all data points satisfy the energy conservation rule fairly well within about a 5% error bound. In the following, another benchmarking hybrid BEM simulation for a sample Lamb wave scattering problem due to a square defect is carried out and compared with the available finite element data (Alleyne and Cawley, 1992). Hence, the same material properties and defect geometry used in the previous work (Alleyne and Cawley, 1992) are employed; the longitudinal wave velocity is 5.96 mm/μs, the transverse wave velocity 3.26 mm/μs and the density 8.0 g/cm^3. The second symmetric Lamb wave mode, A1, interacts with three square defects of different depths of h/d = 1/3, 1/2 and 2/3 under the frequency sweeping condition between fd = 2.3 to 2.6 MHz mm. The plate thickness is fixed as one and other defect geometry parameters, w and h, are readily determined from Fig. 4 for each case.

The transmission factors of the A1 incident mode are calculated by the hybrid BEM code and plotted together with the previous FEM results (Alleyne and Cawley, 1992) in Fig. 5. From the FEM work (Alleyne and Cawley, 1992), the FEM transmission data are blown up and carefully read for use in

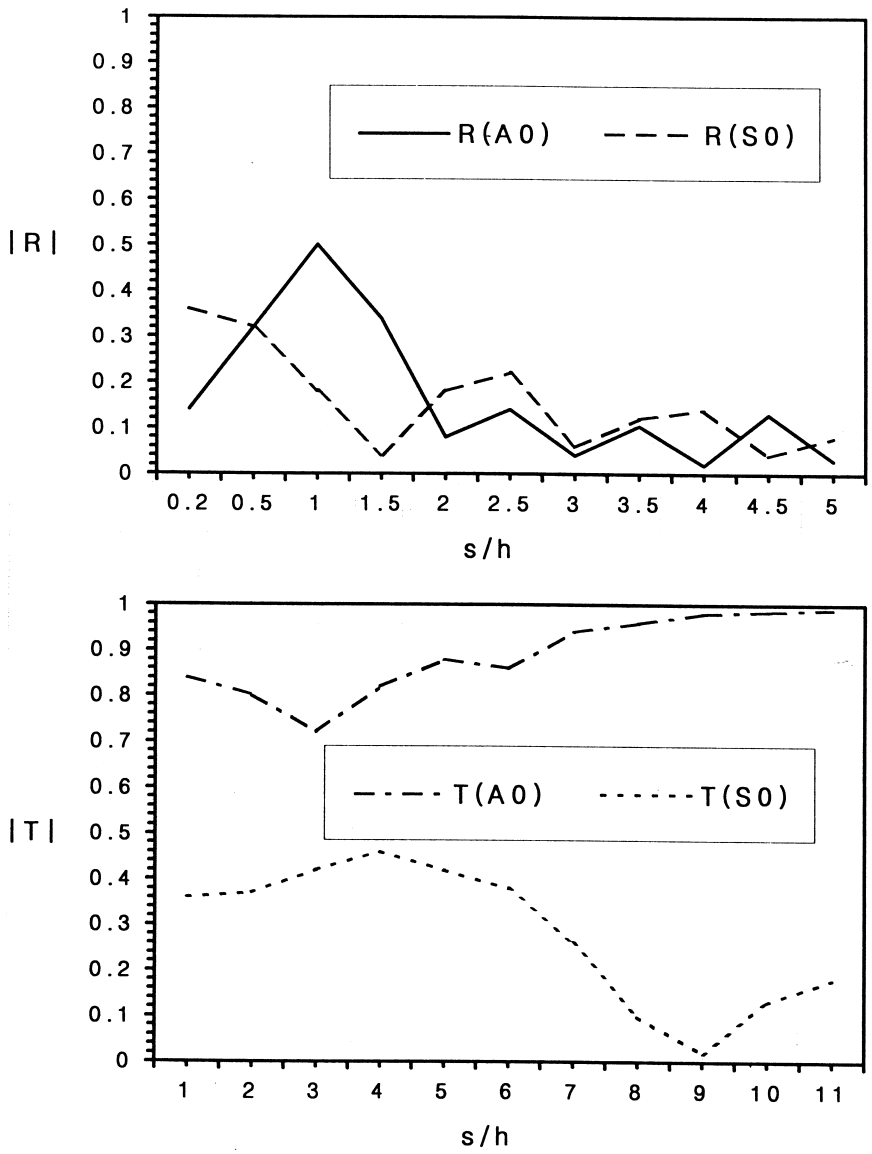

Fig. 7. The variations of reflection and transmission with respect to the aspect ratio change of an elliptical surface defect for A0 (fd = 1.0 MHz mm) incidence (50% depth through the thickness, h = 0.5).

Fig. 5. Because neither the FEM nor the presented BEM data is a closed form solution, rather an approximate numerical solution, the data point can be slightly different in Fig. 5, depending on the mesh profiles, like total number of elements and the way to distribute the elements. There is also some inevitable error in reading the FEM data point from the previous work (Alleyne and Cawley, 1992).

Nevertheless, in Fig. 5, good agreement is achieved in the trend of transmission variation as well as in the direct comparison of each data point between the present hybrid BEM study and the previous FEM work (Alleyne and Cawley, 1992). With about 400 to 500 boundary nodal points along the whole

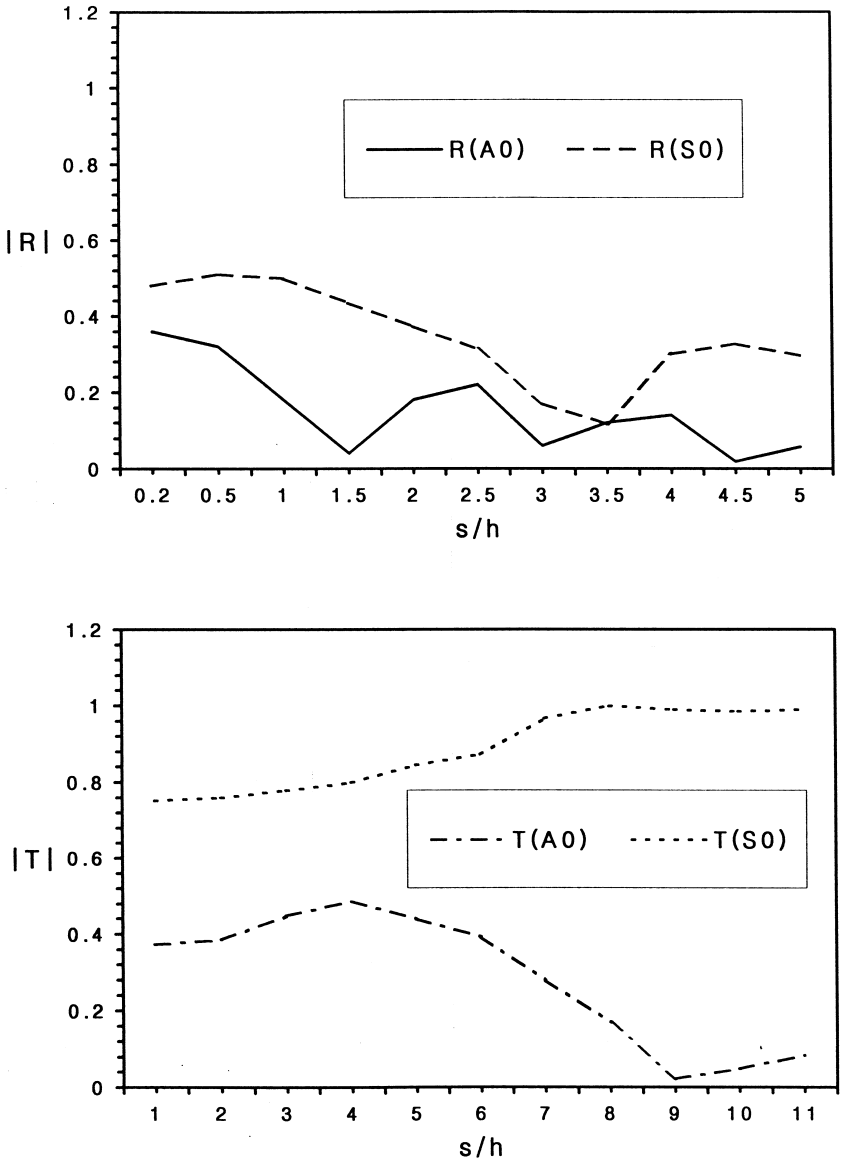

Fig. 8. The variations of reflection and transmission with respect to the aspect ratio change of an elliptical surface defect for S0 (fd = 1.0 MHz mm) incidence (50% depth through the thickness, h = 0.5).

boundary in Fig. 5, the BEM results match quite well with those of the FEM study, reproducing consistently, those key data points like the minima at fd = 2.55 and 2.4 MHz mm for h/d = 1/3 and 1/2, respectively. Through these patch tests, it is shown that the hybrid BEM code developed in this study can be successfully applied to general Lamb wave scattering problems with arbitrary shaped defects with a reasonable error bound.

3.2. The Lamb wave mode conversion studies with respect to defect sharpness

When an incident mode is scattered by a certain type of defect, the incident energy is redistributed into various multi-scattered modes at a given *fd* value on the dispersion curve via a mode conversion phenomena. Reflection and transmission factors obtained by BEM will be plotted with a variation of incident frequencies for various defect shapes in order to find the best change of defect detection by

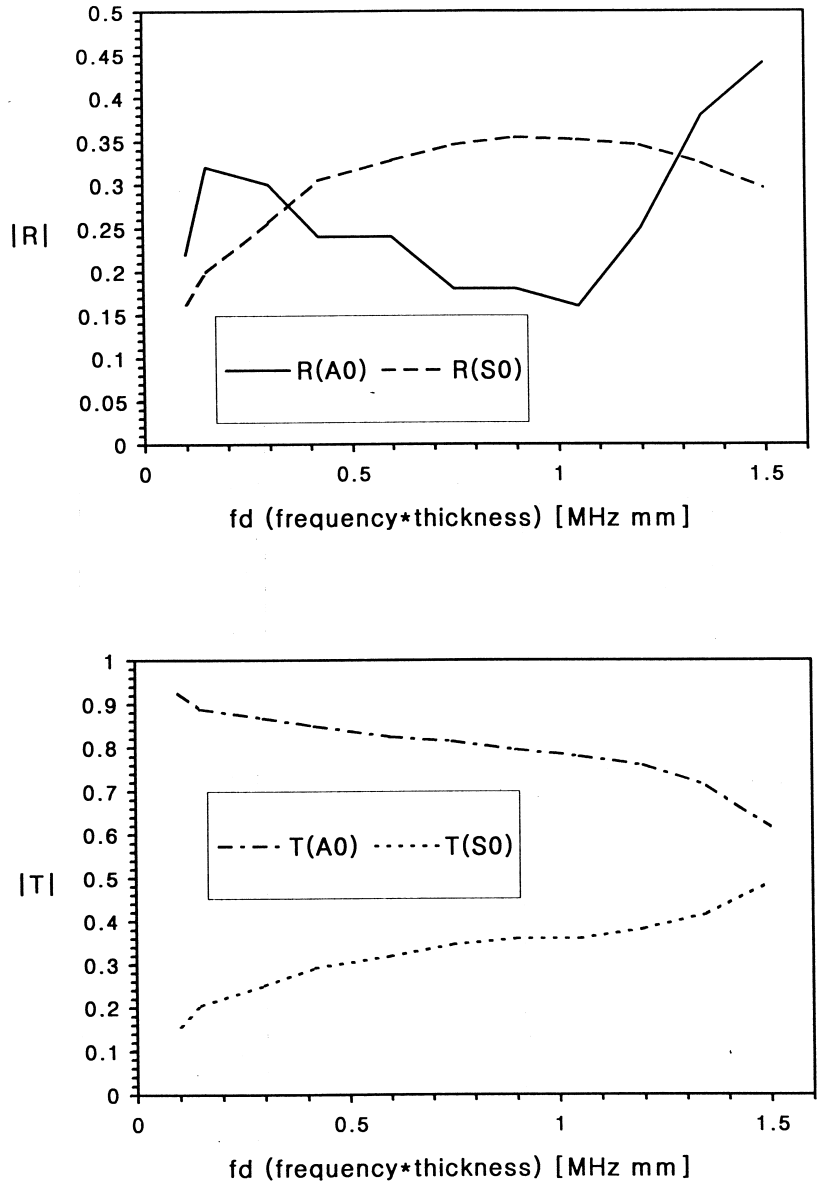

Fig. 9. Variations of reflection and transmission with respect to an incident frequency change for a sharp surface defect (A0 incidence $s/h = 0.2$, $h = 0.5$, 50% depth through the thickness).

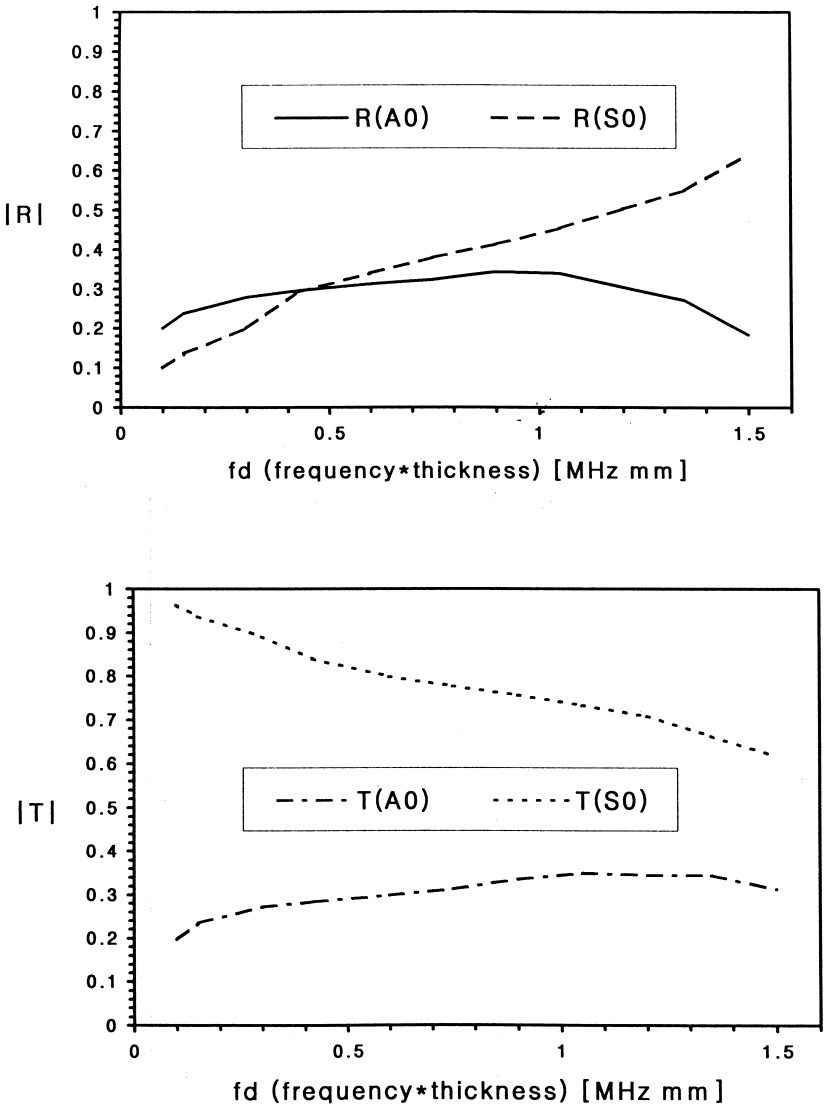

Fig. 10. Variations of reflection and transmission with respect to an incident frequency change for a sharp surface defect (S0 incidence $s/h = 0.2$, $h = 0.5$, 50% depth through the thickness).

greatest changes in mode conversion. The effect of defect sharpness is investigated by changing the aspect ratio of s/h from 0.2 to 5 for a certain incident mode as shown in Fig. 6.

In Fig. 6, s and h denote half of the defect width and depth, respectively. Incident modes, S0 and A0 at $fd = 1.0$ MHz mm are chosen. The defect surface is assumed as an elliptical contour with a different aspect ratio, s/h. This contour can be mathematically defined by the equation of an ellipse and divided with 60 to 70 constant boundary elements while other flat boundaries have 150 to 200 elements. The crack depth is fixed at 0.5, 50% of the waveguide thickness. The BEM results for T (transmission) and R (reflection) of these two modes with respect to s/h are compared with each in Figs. 7 and 8.

At $fd = 1.0$ MHz mm, the incident energy can be scattered backward and forward from a defect,

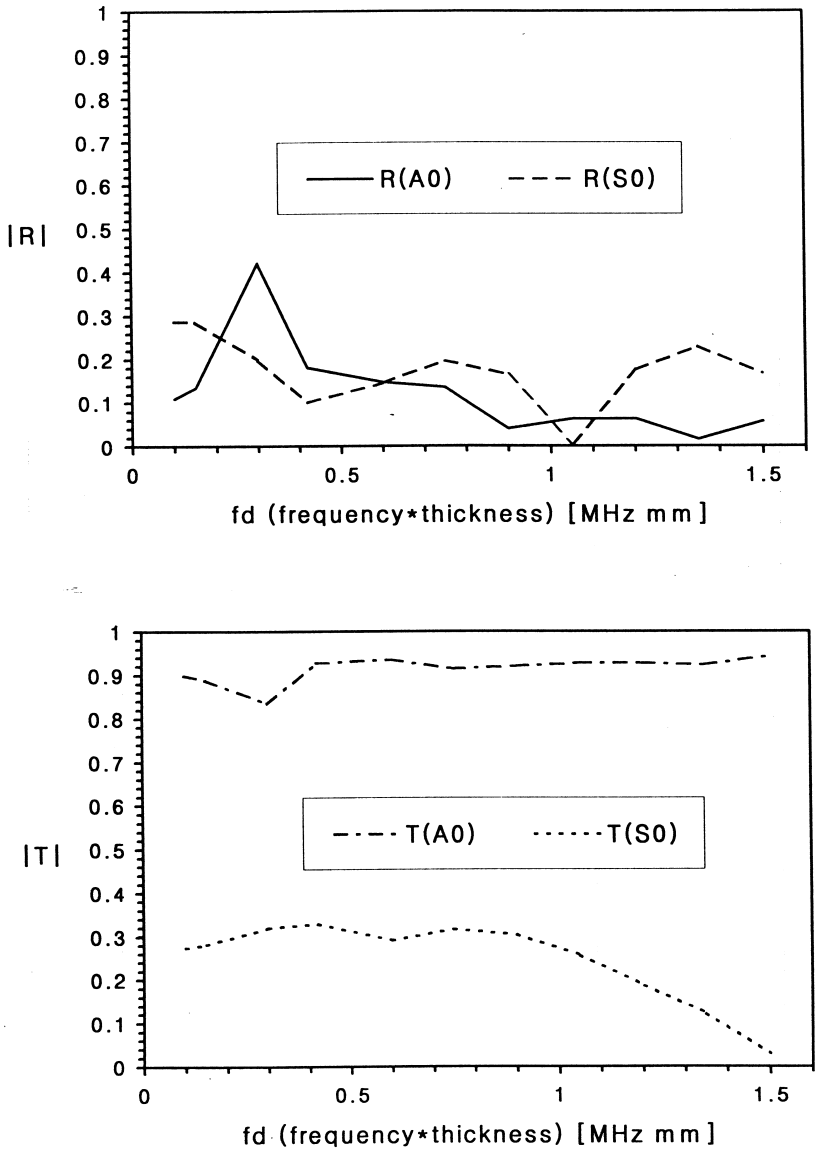

Fig. 11. Variations of reflection and transmission with respect to an incident frequency change for a round surface wastage (A0 incidence $s/h = 3.0$, $h = 0.5$, 50% depth through the thickness).

being associated with only two possible scattered modes, A0 and S0. As shown in Figs. 7 and 8, there is enough variation of R and T with respect to s/h change to be able to select a data acquisition scheme that might be used in classification analysis. In both cases of A0 and S0 incidence, if s/h is bigger than 4.0, the transmission factor of an incident mode is dominant, reaching one, since the mode conversion behavior is expected to become mild due to an increase of crack tip bluntness. Finally, mode conversion converges to a stable stage of a tapered waveguide with smoothly varying thickness in the case of $s/h = 4.0$. Generally speaking, the reflection and transmission of an incident mode show overall the inverse

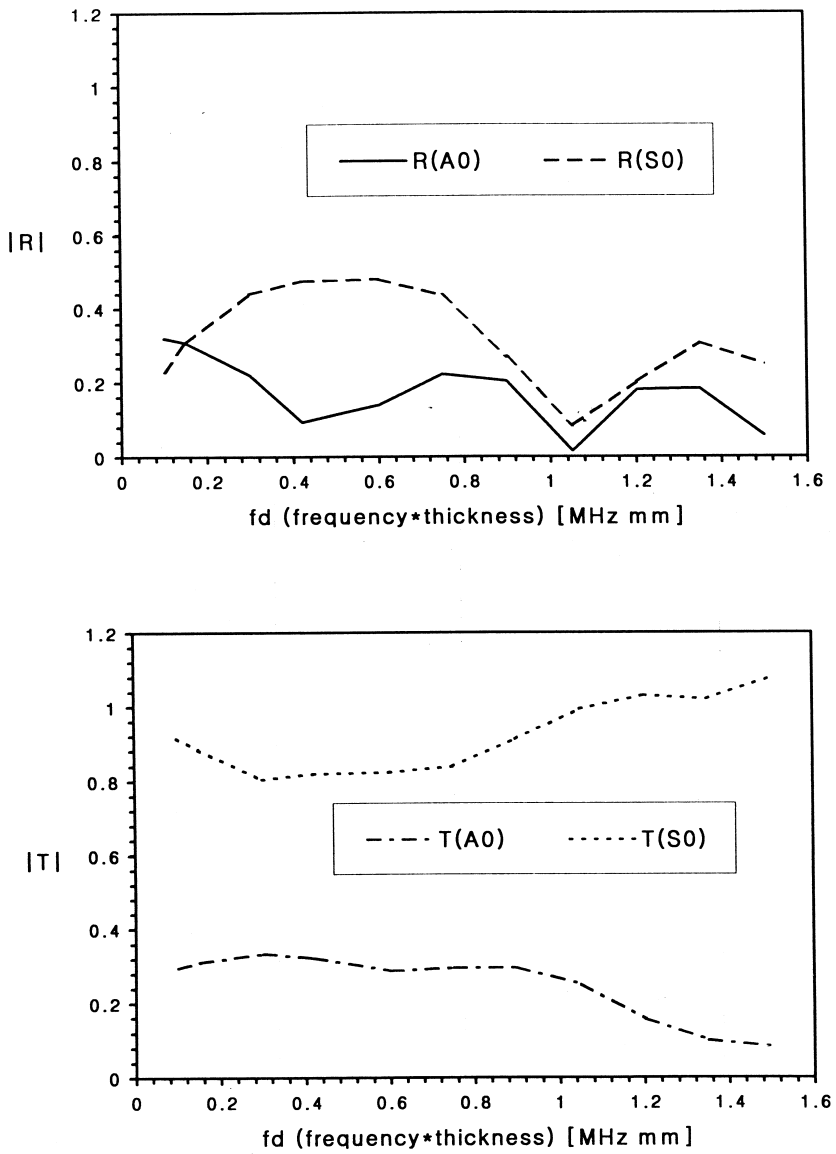

Fig. 12. Variations of reflection and transmission with respect to an incidence frequency change for a round surface wastage (S0 incidence $s/h = 3.0$, $h = 0.5$, 50% depth through the thickness).

trend for energy conservation. It is also observed that the model conversion behavior is overall proportional to defect sharpness. Because each point on the dispersion curves provides a different vibrational pattern; a different displacement distribution, a different mode conversion is expected by a sweeping frequency. Now, incident frequency will be varied between $fd = 0.1$ and 1.5 MHz mm, following two dispersion curves of the incident A0 and S0 modes for a sharp defect and a round wastage with $s/h = 0.2$ and 3.0, respectively. As seen in Figs. 9–12, there is a significant difference in the variations of reflection and transmission factors with an increase of incident frequency between those

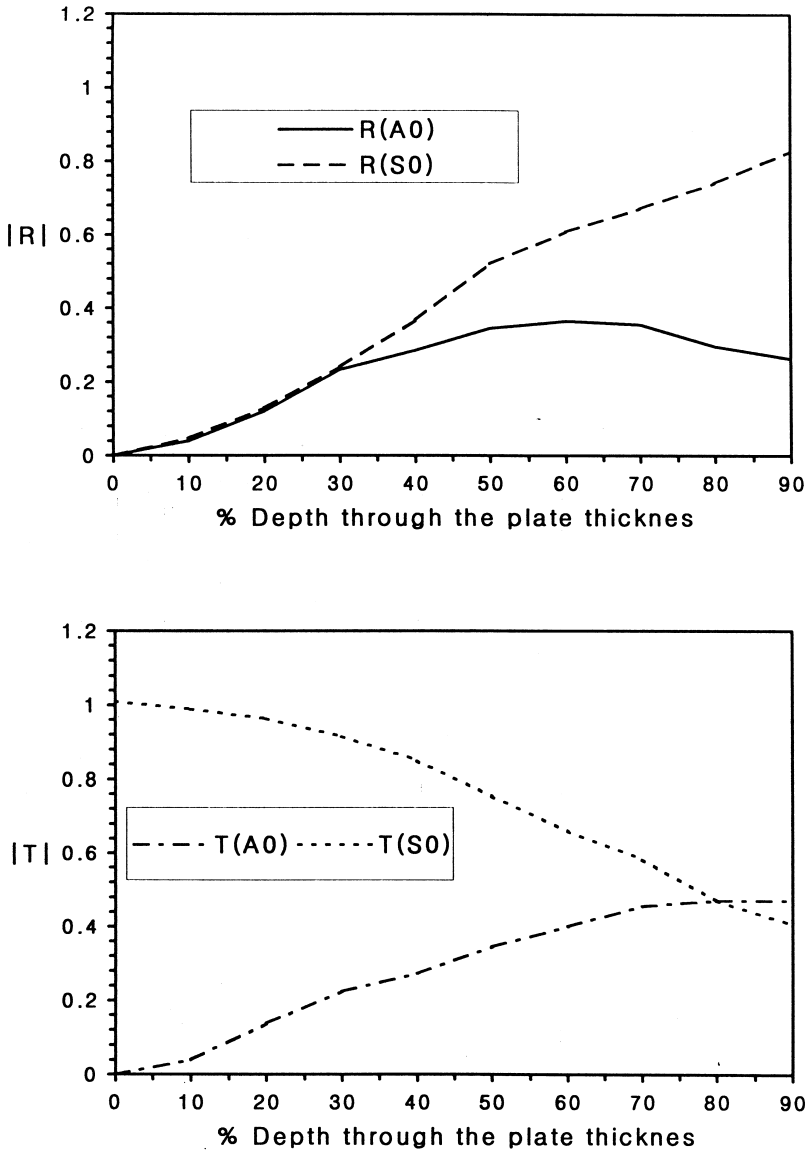

Fig. 13. Variations of reflection and transmission with respect to a depth variation of a sharp surface defect for S0 (fd = 1.0 MHz mm) incidence (s = 0.05, d = 1.0).

two different defects with s/h = 0.2 and 3.0, respectively. For a sharp defect with s/h = 0.2 subjected to S0 incidence, the incident S0 mode transmission and reflection monotonically decreases and increases, respectively, with an fd increase, as shown in Fig. 10, whereas the A0 incidence shows only slight changes in Fig. 9. For a round defect with s/h = 3.0, in the case of the S0 incidence, the transmission and reflection of the incident mode, S0, are dominant over the entire frequency sweeping range in Fig. 12. However, compared to Fig. 10, the trend is quite different from the case of a sharp defect. In Fig. 12, the transmission and reflection of the S0 mode have minimum and maximum sensitivities, respectively, around fd = 0.6 MHz mm showing nearly the parabolic variation up to fd = 1.0 MHz mm.

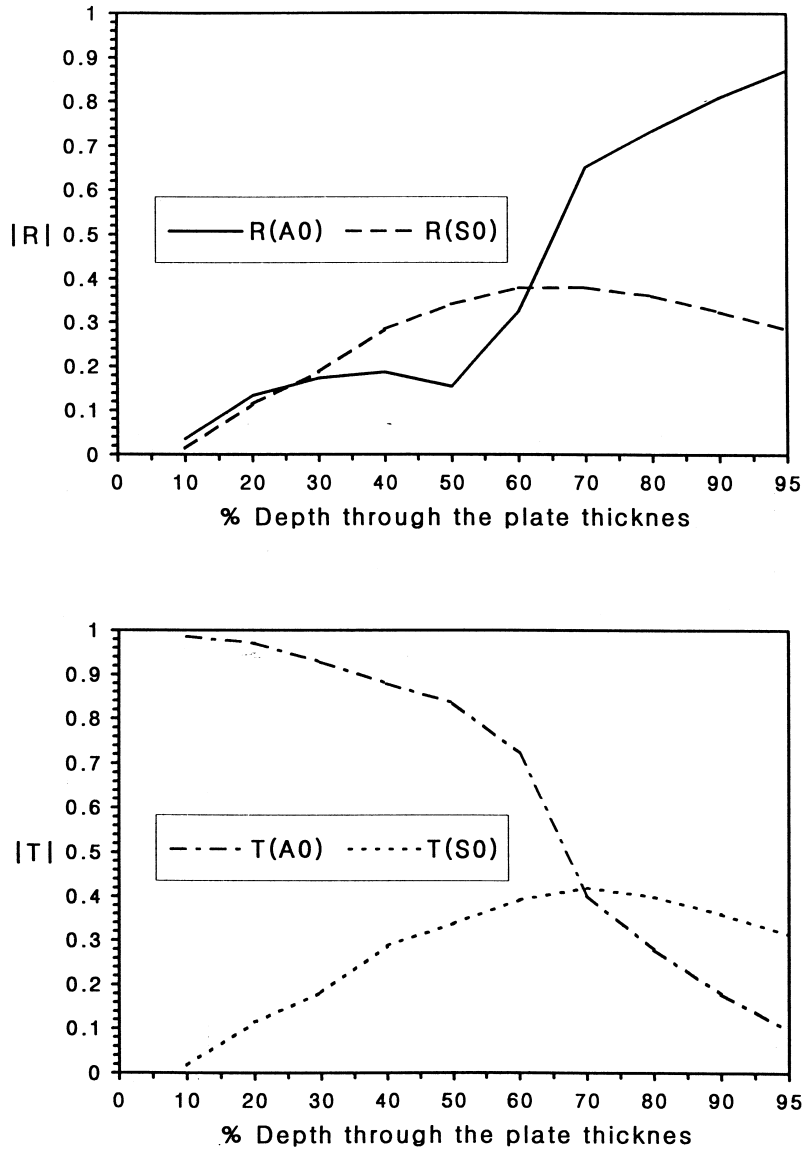

Fig. 14. Variations of reflection and transmission with respect to a depth variation of a sharp surface defect for A0 (fd = 1.0 MHz mm) incidence (s = 0.05, d = 1.0).

Consequently, variations of reflection and transmission of an incident mode are quite different depending on both defect sharpness and incident mode selection, whereas those of the minor modes are mostly affected by only defect sharpness. For example, forward and backward scattering behaviors of secondary modes like S0 and A0 incidence and A0 from S0 incidence are very similar to each other; despite the incident mode difference between A0 and S0 in both cases of a sharp defect and a round wastage. However, there is a remarkable change depending on defect sharpness between s/h = 0.2 and 3.0, as seen in Figs. 9 and 11 and Figs. 10 and 12.

3.3. The Lamb wave mode conversion studies with respect to defect depth

A sharp defect with $s = 0.05$ subjected to either A0 or S0 incidence at $fd = 1.0$ MHz mm is chosen for the defect depth study. The defect depth varies between $h/d = 0.1$ and 0.9. Figs. 13 and 14 show the reflection and transmission for both primary (incident) and secondary (converted) modes under S0 and A0 incidence, respectively. As seen in Figs. 13 and 14, reflection and transmission for a secondary mode monotonically increase with defect depth, because the larger reflector surface creates more mode conversion. However, after reaching their maximum, the secondary mode scatterings show a tendency to decrease with respect to an increase of defect depth. Since the problem converges to the edge reflection subjected to an incident model, it generates only the incident mode reflection due to the symmetric reflection. Maximum mode conversion occurs when a sharp defect propagates up to about 65% of wall thickness, in both cases of A0 and S0 incidence.

4. Conclusions

Hybrid BEM based on a combination of the elastodynamic interior boundary integral equation and the normal mode expansion technique were applied to a study of Lamb wave scattering due to surface defects. Numerical details on a hybrid formulation were also discussed. The accuracy of the hybrid BEM formulation on the guided wave scattering problems was satisfactory in terms of energy conservation; the BEM patch test results also show good agreement with the benchmarking FEM data. It turns out that the hybrid BEM can successfully solve the multi-mode conversion phenomena found in a guided wave scattering problem. The present method is also capable of handling a geometrical discontinuity in a more efficient manner over a domain type technique. Finally, the guided wave scattering data can be obtained as a function of defect sharpness, depth, incident mode and frequency. Based on a unique scattering pattern from a defect predicted by the BEM, guided wave potential for defect characterization study was explored.

Acknowledgements

The authors wish to acknowledge the partial financial support of the Korea Research Foundation made in the program year of 1997 under Contract No. 1997-003-E00035 and Inje University in the program year of 1997. A special thank is also to the Electrical Power Research Institute and to the office of Naval Research for their financial support.

References

Achenbach, J.D., 1975. Wave Propagation in Elastic Solids. Elsevier, New York.

Achenbach, J.D., 1992. Mathematical modeling for quantitative ultrasonics. Nondestr. Test. Eval. 8 (9), 363–377.

Alleyne, D.N., Cawley, P., 1992. The interaction of Lamb waves with defects. IEEE Transactions on Ultrasonics, Ferroelectrics, and Frequency Control 39 (3), 381–397.

Al-Nassar, Y.N., Datta, S.K., Shah, A.H., 1991. Scattering of Lamb waves by a normal rectangular strip weldment. Ultrasonics 29, 125–132.

Auld, B.A., Tsao, E.M., 1977. A variational analysis of edge resonance in a semi-infinite plate. IEEE Transactions on Sonics and Ultrasonics 24 (5), 317–326.

Bond, L.J. 1990. Numerical techniques and their use to study wave propagation and scattering—a review. In: Elastic Waves and Ultrasonic Nondestructive Evaluation. North-Holland, pp. 17–27.

Brebbia, C.A., Tells, J.C.F., Wrobel, L.C., 1984. Boundary Element Techniques. Springer, Berlin.
Brebbia, C.A., Umetani, S., Trevelyan, J. 1985. Critical comparison of boundary element and finite element methods for stress analysis, BETECH 85. In: Proceedings of the 1st Boundary Element Technology Conference, South Australian Institute of Technology, Adelaide, Australia, pp. 225–256.
Cho, Y., Rose, J.L., 1996a. Guided waves in a water loaded hollow cylinder. Nondestr. Test. Eval. 12, 323–339.
Cho, Y., Rose, J.L., 1996b. A boundary element solution for a mode conversion study on the edge reflection of Lamb waves. Journal of the Acoustical Society of America 99 (4), 2097–2109.
Datta, S.K., Al-Nassar, Y., Shah, A.H., 1991. Lamb wave scattering by a surface breaking cracks in a plate. Review of Progress in Quantitative Nondestructive Evaluation 10A, 97–104.
Karim, M.R., Awal, M.A., Kundu, T., 1992. Elastic wave scattering by cracks and inclusions in plates: in-plane case. Int. J. Solids Structures 29 (19), 2355–2367.
Kitahara, M., Nakagawa, K., Achenbach, J.D., 1989. Boundary-integral equation method for elastodynamic scattering by a compact inhomogeneity. Computational Mechanics 5, 129–144.
Kobayashi, S. 1987. Chapter 4 elastodynamics. In: Boundary Element Methods in Mechanics. North-Holland, New York, pp. 192–255.
Koshiba, M., Karakida, S., Suzuki, M., 1984. Finite-element analysis of Lamb waves scattering in an elastic plate waveguide. IEEE Transactions on Sonics and Ultrasonics 31 (1), 18–25.
Lachat, J.C., Watson, J.O., 1976. Effective numerical treatment of boundary integral equations: a formulation for three-dimensional elastostatics. International Journal for Numerical Methods in Engineering 10, 999–1005.
Lamb, H. 1889. The flexure of an elastic plate. In: Proceedings of the London Mathematical Society, pp. 85–90.
Lancaster, P., Tismenetsky, M., 1985. The Theory of Matrices, 2nd ed. Academic Press, Orlando.
Rezayat, M., Shippy, D.J., Rizzo, F.J., 1986. On time-harmonic elastic-wave analysis by the boundary element method for moderate to high frequencies. Computer Methods in Applied Mechanics and Engineering 55, 349–367.
Rizzo, F.J., Shippy, D.J., Rezayat, M., 1985. A boundary integral equation method for radiation and scattering of elastic waves in three dimensions. International Journal for Numerical Methods in Engineering 21, 115–129.
Rokhlin, S., 1980. Diffraction of Lamb waves by a finite crack in an elastic layer. Journal of the Acoustical Society of America 67 (4), 1157–1165.
Rose, J.L., Rajana, K.M., Carr, F.T., 1994. Ultrasonic guided wave inspection concepts for steam generator tubing. Materials Evaluation 52 (2), 307–311.
Schafbuch, P.J., Thompson, R.B., Rizzo, F.J., 1993. Elastic scatterer interaction via generalized Born series and far-field approximations. Journal of the Acoustical Society of America 93 (1), 295–307.
Talbot, R.J., Przemieniecki, J.S., 1975. Finite element analysis of frequency spectra for elastic waveguides. Int. J. Solids Structures 11, 115–138.
Viktorov, I.A., 1967. Rayleigh and Lamb Wave: Physical Theory and Applications. Plenum Press, New York.
Zhang, C.H., Achenbach, J.D., 1988. Scattering by multiple crack configurations. Transactions of the ASME 55, 104–110.
Zhang, S.Y., Shen, J.Z., Ying, C.F., 1988. The reflection of the Lamb wave by a free plate edge: visualization and theory. Materials Evaluation 46, 638–641.